Power Management Strategy Based on Virtual Inertia for DC Microgrids

Neto, Pedro Jose Dos Santos; Barros, Tarcio Andre Dos Santos; Silveira, Joao Pedro Carvalho; Filho, Ernesto Ruppert; Vasquez, Juan Carlos; Guerrero, Josep M.

Published in:
IEEE Transactions on Power Electronics

DOI (link to publication from Publisher):
10.1109/TPEL.2020.2986283

Publication date:
2020

Document Version
Accepted author manuscript, peer reviewed version

Power Management Strategy Based on Virtual Inertia for DC Microgrids

Pedro José dos Santos Neto, *Student Member, IEEE*, Tárcio André dos Santos Barros, *Member, IEEE*, João Pedro Carvalho Silveira, *Student Member, IEEE*, Ernesto Ruppert Filho, *Member, IEEE*, Juan Carlos Vasquez, *Senior Member, IEEE*, and Josep M. Guerrero, *Fellow, IEEE*

***Abstract*—This paper presents a power management strategy (PMS) to control the power flow in a DC microgrid operating in the grid-connected mode. The microgrid model is composed of the AC utility grid interfaced with a voltage source inverter operating as a grid-forming converter (VSC), an energy storage system (ESS) formed by a battery bank and a bidirectional DC-DC converter operating as a grid-supporting unit, a distributed generation acting as a grid-feeding unit, and the customer loads with strict voltage regulation. The power management technique applies a virtual inertia concept together with a state of charge-based management function to regulate the charging and discharging process of the battery bank according to the DC microgrid power flow. Thus, high-rate peaks of power are avoided, which improves the ESS life cycle. With the proposed PMS, an autonomous power flow is achieved inside the DC microgrid, while the AC utility grid focuses exclusively upon forming the DC bus and processing the surplus or shortage of power. In addition, the proposed strategy simplifies the communication link between the grid inverter and the ESS, since the VSC power is the sole information exchanged. The experimental results show that the proposed PMS is reliable, leading to high ESS performance and power flow control within the DC microgrid, without degrading the DC bus voltage.**

***Index Terms*—DC microgrid, power management strategy, energy storage system, virtual inertia, grid-connected mode.**

NOMENCLATURE

CPL Constant Power Load
DG Distributed Generation
ESS Energy Storage System
IGBT Insulated Gate Bipolar Transistor
LPF Low Pass Filter
PMS Power Management System
PWM Pulse Width Modulation
SOC State of Charge
VI Virtual Inertia
VSC Voltage Source Converter

Variables:
C_{bus}, C_{dg}, C_{ess}, C_l - Capacitance of power converters [F]
C_{nom} - Battery nominal capacity [C]
d_{ess}, d_{dg}, d_l, d_{vsc} - Duty cycle of power converters
D_l, D_{dg} - Diodes used in power converters
D_m, D_p - Damping factor [N.m.s/rad]
E_B - Internal battery bank voltage [V]
e_{idg}, e_{id}, e_{iq}, e_p, e_{vbus}, e_{vess}, e_{vl}, e_{iess} - Control errors
f_{swdg}, f_{swess}, f_{swl}, f_{swvsc} - Switching frequencies [Hz]
i_{dg}, i_{ess}, i_{load}, i_{vsc} - Currents of power converters [A]
I_d, I_q - VSC dq currents [A]
I_{dref}, I_{qref}, $I_{dg,ref}$, $I_{ess,ref}$ - Current references [A]
J_m, J - Virtual inertia coefficient [kg.m^2]
k_{pi}, k_{pv}, k_{piB}, k_{iiB} - PI parameters of the VSC and ESS
k_{pd}, k_{id}, k_{pl}, k_{il} - PI parameters of the DG and load
L_{ess}, L_{vsc}, L_{dg}, L_l - Inductance of the converters [H]
m_d, m_q, m_a, m_b, m_c - VSC modulation indexes
$M1$, $M2$ - ESS mode 1 and mode 2
P_{Bref} - ESS power reference [W]
P_{dg}, P_{ess}, P_{load}, P_{vsc} - Converters average power [W]
P_{loss} - Power losses inside the microgrid [W]
P_{ref}, Q_{ref} - VSC active [W] and reactive [VAr] power references
P_s, Q_s - Active [W] and reactive [VAr] power control input
P_{ext}, P_t - VSC AC external and terminal power [W]
R_{load} - Load resistance [Ω]
soc_a, soc_b, soc_{min}, soc_{max} - ESS state of charge limits
S_{b1}, S_{b2}, S_{dg}, S_l, S_{v1a}, S_{v2a}, S_{v3a}, S_{v1b}, S_{v2b}, S_{v3b} - IGBT switches used in power converters
SOC_0 - Initial state of charge
T_m, T_e - Mechanical and electromagnetic torque [N.m]
V_{bus} - DC bus voltage [V]
V_d, V_q - VSC dq voltages [V]
V_{dg}, V_{ess}, V_{load}, V_{bus} - Voltages of power converters [V]
V_{ref}, V_{busref}, V_{lref} - Voltage references of converters [V]
$V_{3\phi}$, $I_{3\phi}$ - 3-phase voltage [V] and current [A] of AC grid
Z_B - Battery internal impedance [Ω]
z_0, z_1, p_0, p_1, p_2, p_3, p_4 - Zeros and poles of the PMS open loop transfer function
θ_S - AC grid synchronism angle [º]
ω_1, ω_2, ω_3, ω_4 - Cutoff frequencies of the LPFs [rad/s]
ω - Angular velocity [rad/s]
Δp - PMS power mismatch [W]
ψ - SOC based function

Manuscript received September 30, 2019; revised November 18, 2019; accepted March 24, 2020.

This work was supported by the São Paulo Research Fundation, FAPESP, grant numbers 16/08645-9, 17/21087-8, 17/21640-9, and 18/22076-2.

J. M. Guerrero and J. C. Vasquez were funded by a Villum Investigator grant (no. 25920) from The Villum Fonden.

P. J. dos Santos Neto, J. P. C. Silveira and E. Ruppert Filho are with the School of Electrical and Computer Engineering, University of Campinas, Campinas, 13083-852, São Paulo, Brazil (e-mail: pedro_jsn@outlook.com, jpedro.carvalhosilveira@gmail.com, ruppert@fee.unicamp.br).

T. A. S Barros is with the Faculty of Mechanical Engineering, University of Campinas, 13083-860, São Paulo, Brazil (e-mail: tarcioandre@fem.unicamp.br).

J. C. Vasquez and J. M. Guerrero are with the Center for Research on Microgrids (CROM), Department of Energy Technology, Aalborg University, 9220 Aalborg East, Denmark (e-mail: juq@et.aau.dk, joz@et.aau.dk).

Color versions of one or more of the figures in this paper are available online at http://ieeexplore.ieee.org.

I. Introduction

Due to the evolution of power electronics over the last years, DC microgrids have been pointed out as an alternative solution for smart grid systems, as these structures present clear advantages over the conventional AC microgrids [1]–[3]. Among these advantages, one can mention lower losses due to reduction of conversion steps, no skin effect, the absence of reactive power, and the control simplicity because only active power flows inside the microgrid. Moreover, the increasing demand of DC electronic loads warms up the discussion about a generation using direct current. In addition, appealing for renewable energy insertion favors DC applications, since a DC step conversion is commonly used to control intermittent energy sources in solar or variable speed wind systems [4]–[6].

The control and management of the DC microgrids are the main concerns of researchers. Droop control and its variants have as advantages the simplicity of implementation and the absence of any communication link between the power electronic converters [7], [8]. However, droop control imposes a DC bus voltage variation and current sharing mismatch depending on the droop parameter choice [8]–[10]. The hierarchical control, in its turn, aims to correct these mismatches by adding a secondary and upper layers of control [9], [11]–[13]. The secondary control requires a low bandwidth communication line for a central control system or, alternatively, can be designed in a distributed fashion [14]–[18].

Adaptive droop is usually employed to achieve a state of charge (SOC) dependent behavior of the energy storage system (ESS). In the methods presented in [3], [13], [19]–[21], the droop coefficient varies as a function of the state of charge of the energy storage system, which adaptively controls the output voltage. The cited methods are predominantly applied to regulate power sharing among multiple ESSs. Nevertheless, the variation of the droop characteristic with the state of charge does not result in a full control over the ESS output power. Therefore, the DC microgrid power flow is compromised.

Droop control is especially useful for the island mode operation, in which the distributed generation (DG) and the ESS are presented. However, considering an urban distribution system, an operation in the island mode is seldom expected; as consequence, the microgrid should be working in the grid-connected mode for the vast majority of the time during normal conditions. For an urban DC microgrid in the grid-connected mode, a conventional droop control forces the ESS to share the power flow with the AC utility grid. Nonetheless, if autonomous operation is desired, the microgrid has to rely on the ESS and the DGs to provide the power required by customer loads. That means the AC utility grid absorbs or injects power when the other sources are not able to maintain the power flow. Hence, a proper investigation of the control and management methods of the DC microgrid in the grid-connected mode must be conducted.

DC microgrids present a known low inertia nature due to the presence of many power electronic converters applied to control the energy storage system, loads, and distributed generation. This absence of inertia causes problems in the DC bus voltage stability, mainly when constant power loads (CPL) are being supplied in the island mode [22]–[24]. In an autonomous grid-connected mode, when the ESS is working to maintain the power flow stability and the utility grid is used as a backup, the problem of the low inertia particularly affects the battery bank. This occurs because, without the inertia, the ESS may be submitted to rapid power variations, which increases the battery failure rate and contributes to reduce their life cycle [25]–[27]. As pointed out in [26], [28], [29] an uncontrolled high-rate charge or discharge operation results in an irreversible battery damage. A possible solution is to use hybrid ESS arrangements, in which high power density devices such as supercapacitors are managed to generate fast power variations, while the battery bank is managed to supply the low frequency power imbalances [25], [30]–[34]. This method, however, increases the cost and control complexity of the energy storage system.

Virtual inertia (VI) strategies have been studied as an alternative to improve the low inertia nature of DC microgrids [27], [35]–[41]. In [37], a VI control emulating a synchronous machine is proposed to improve the fluctuation response of the DC bus voltage. This method is applied in the grid converter control of the DC microgrid, which makes it suitable for grid-connected operation. However, only the voltage fluctuation is the object of analysis; no ESS power management is considered. A similar VI strategy is used in [36]. The authors suggest the VI control at the grid converter together with an improved dual droop control and a power system stabilizer in order to achieve frequency regulation and an enhanced DC microgrid stability. The proposed VI strategy is not incorporated in the energy storage management system and the droop control drawbacks are part of the applied grid-connected mode. A coordinated control for DC microgrids based on bus-signaling and VI is presented in [35]. A proper management strategy is considered by the authors and the VI concept is applied to the renewable energy sources. Nevertheless, the grid-connected mode is not considered. In [27], a VI control is applied for photovoltaic arrays to improve the dynamic performance of the DC microgrid. An adaptive gain is used to ensure the power sharing between the photovoltaic arrays. In this case, the VI strategy has no integration to the energy storage system and only the island mode is analyzed.

A VI synthesis allied with predictive control is proposed for DC microgrids in [41]. The method defended by the authors enables adaptive synthetic inertia, which is claimed to stabilize the DC bus voltage in case of disturbances. One more time, this strategy is focused only on the island mode, and no energy storage system is considered. The concept of a virtual DC machine is introduced by [38], in which the dynamics of a DC machine are emulated at the bidirectional DC-DC converter control of the ESS. The inertia of a DC machine is emulated to achieve stable operation and smoothness voltage variation during transients. It is worth mentioning, however, that only simulation results are presented by the authors. In addition, grid-connected mode is not investigated and no energy storage management system is incorporated in the proposed technique. The grid-connected mode is adopted in [39], in which a VI control is employed to regulate the

frequency of the AC side in the presence of AC load and wind speed variations; a supercapacitor ESS is part of the inertia improvement proposal. Nonetheless, the study focuses on wind systems in microgrids, only simulation results are presented, and no ESS management function is incorporated. An inertia emulation technique is proposed in [40] for DC microgrids supplying AC loads. The authors propose voltage regulation and frequency regulation by means of a virtual excitation. A power management system is applied to coordinate the current sharing between the grid and the ESS. Notwithstanding, the VI is not integrated with the PMS and only simulation results are presented.

Considering the drawbacks of previous research in this field, this paper proposes a power management strategy (PMS) to guarantee autonomous operation of a DC microgrid in the grid-connected mode. A virtual inertia concept is introduced at the ESS control to guarantee flexible regulation over the power flow transient response. A state of charge management function is integrated to the VI system to obtain power adaptive behavior, avoiding the high-rate charge/discharge and thus improving the battery bank life cycle. The objective is to achieve stable power flow, taking into account the ESS state of charge limitations. The strategy under study does require communication between the converters. However, only the power information is exchanged from the voltage source converter to the ESS unit, which simplifies the communication procedure. Experimental results are conducted to validate the proposed methodology.

This paper is structured as follows. Section II presents the studied DC microgrid, including the considered elements of an urban distribution system. Section III details the proposed power management strategy, including the main considerations about the virtual inertia and the SOC management function. Section IV contains the modeling of the DC microgrid elements and its respective control design. Section V presents an analysis of the proposed PMS by considering the effect of the inertia parameters over the stability and behavior of the system. Section VI discusses the experimental results in detail. Finally, the conclusions are summarized in Section VII.

II. DC MICROGRID DESCRIPTION

The microgrid examined in this paper consists of the energy storage system, the main AC utility grid, the distributed generation, and the customer load, as depicted in Fig. 1. Power electronic converters are responsible for guaranteeing the desirable power flow, voltage, and frequency regulation through the microgrid. Each component's considerations are given in the following subsections.

1) Energy storage system: An energy storage system based on a 240 V battery bank is connected to the DC bus by means of a bidirectional DC-DC converter, which allows for both charging and discharging operations. The ESS rated power is 1 kW and the behavior of the ESS is limited by the battery bank state of charge. When the battery bank is fully charged, the DG surplus power has to run through the VSC into the AC grid, as the ESS cannot absorb this energy. On the other side, if the inferior SOC level is reached, then the ESS must not inject any more power, and the AC grid starts to support the load requirements together with the DG. This action is implemented by using a SOC-based management function. A virtual inertia control is employed to regulate the ESS transient response by adding inertia to the system.

2) AC utility grid: A 3-phase, 60 Hz, 220 Vrms line-to-line utility grid coupled with a 2.2 kW voltage source converter (VSC) is employed to form the DC bus. In this configuration, the VSC works as a grid-forming converter. The DC bus voltage level is set at 400 V to match the VSC conversion requirements for the respective AC utility grid. The ultimate goals of the VSC are to keep the DC bus voltage constant and to allow the power flow stability, which means that the VSC works mainly as an active rectifier. The power management strategy used in this paper forces the AC grid to act only in the transient period, as a backup system, while the ESS must work to guarantee the power flow for the DG and load power variations.

3) Distributed generator: The distributed generator is modeled as a current source able to inject up to 1 kW of active power into the system when required. As the main power source, the DG-rated power is considered as the rated power of the microgrid under analysis. Although renewable energy sources are generally preferable as the DG, this model does not consider the particularities of any renewable system, since only the power flow is under investigation. It is assumed that a solar system or a variable speed wind system should function based on the tracking of the maximum power point. The DG converter guarantees the stable operation considering the intermittent characteristics of a renewable power source.

4) Customer loads: The DC loads are implemented by a step-down DC-DC converter supplying a 1 kW resistive load. The load voltage is tightly regulated at 127 V. This is done to model the behavior of a constant power load (CPL), in which the load presents a negative impedance characteristic, which may lead the system to instability and DC voltage collapse [22]–[24].

III. PROPOSED POWER MANAGEMENT STRATEGY

The proposed power management technique is a centralized control, i.e. a high-speed communication link between the converters is required. For a DC nanogrid, as the one studied in this paper, the categories of consumer's premise communication such as the home area network (HAN), building area network (BAN), or industrial area network (IAN) are best suited for this study. These networks are able to cover an area up to 100 m, with a data rate up to 100 kbps, ideal for receiving signals from energy/power management systems. The main technologies in this field are PLC, Bluetooth, Ethernet, ZigBee, and Wi-Fi [2], [42], [43]. The details and specifications of a particular technology are not the focus of this study.

In the proposed PMS, the voltage source converter acts as a grid-forming unit, while the others are controlled as grid-supporting or grid feeding-converters. As detailed in Fig. 1, the VSC active power flow is measured (detail G) and transmitted to be used in the PMS of the ESS control (detail A). Thus, the

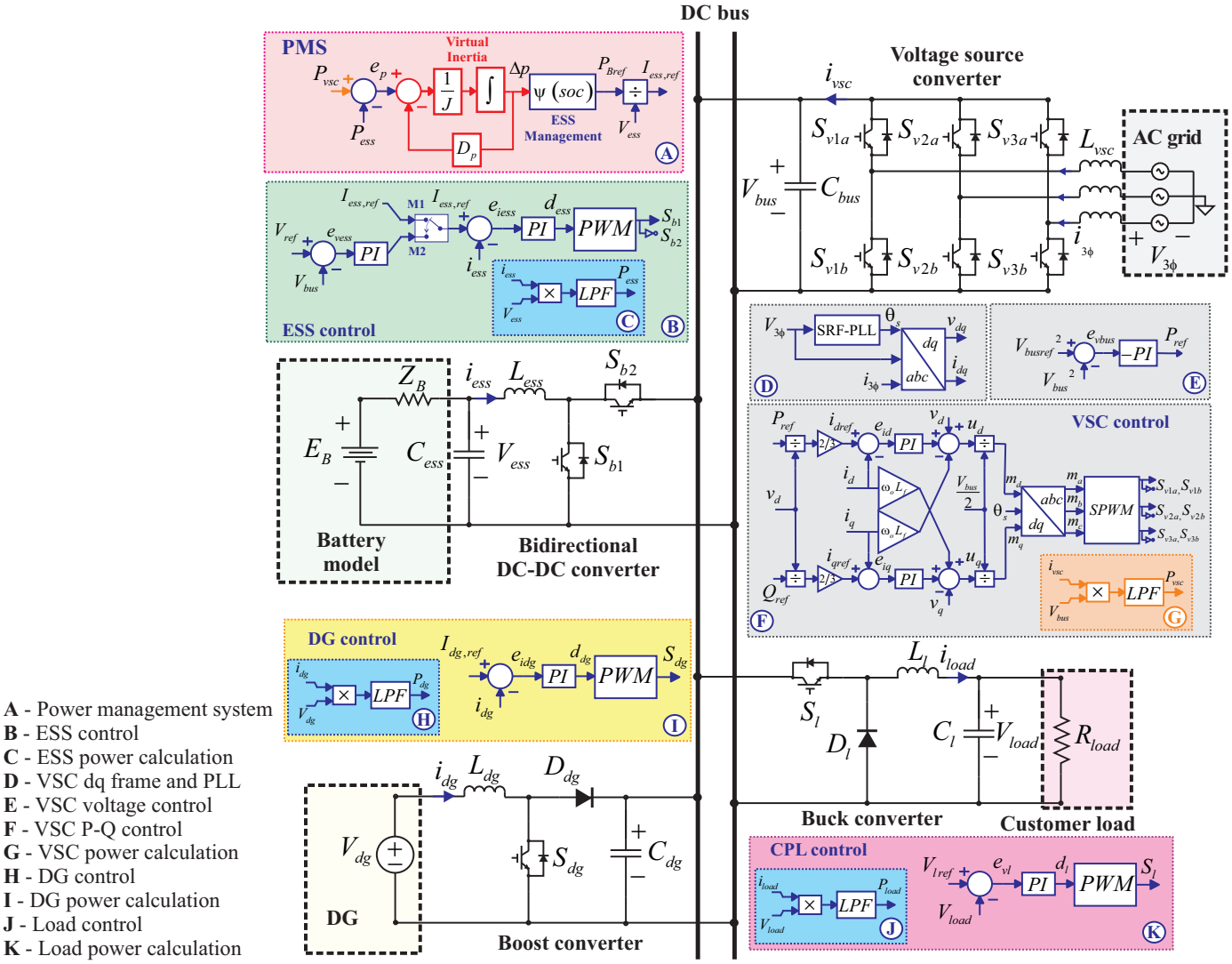

Fig. 1. Detailed overview of the DC microgrid under study. Power electronic converters are depicted in black, and their respective control systems are presented in dark blue. The orange color represents the communication link exchange of information. The ESS virtual inertia is highlighted in red. Line impedances were omitted for the sake of simplification.

ESS acts as a grid-supporting converter. The DG converter acts by tracking the maximum power point and injecting power as a grid-feeding unit.

A. Power flow analysis

To compute the power flow inside the DC microgrid, the average power of the ESS, P_{ess}, distributed generator, P_{dg}, load, P_{load}, and VSC, P_{vsc}, according to the details C, H, J, and G of Fig. 1, are given respectively by:

$$P_{ess} = (V_{ess} \times i_{ess}) \left(\frac{\omega_1}{s + \omega_1} \right) \quad (1)$$

$$P_{dg} = (V_{dg} \times i_{dg}) \left(\frac{\omega_2}{s + \omega_2} \right) \quad (2)$$

$$P_{load} = (V_{load} \times i_{load}) \left(\frac{\omega_3}{s + \omega_3} \right) \quad (3)$$

$$P_{vsc} = (V_{bus} \times i_{vsc}) \left(\frac{{\omega_4}^2}{s^2 + 2\zeta\omega_4 s + \omega_4^2} \right) \quad (4)$$

where V_{ess} and i_{ess} are the energy storage system voltage and current, V_{dg} and i_{dg} are the distributed generator voltage and current, V_{load} and i_{load} are the load voltage and current, V_{bus} and i_{vsc} are the VSC DC bus voltage and current, ω_1, ω_2, ω_3, ω_4 are the cutoff frequency of the low pass filters (LPF) of each converter, and ζ is the damping factor of the VSC second order filter.

A second order filter is used to obtain the average active power of the VSC, as this element controls the DC voltage link. Thus, it is essential to mitigate the voltage and current ripples with higher order filters before sending power information through the communication line. The values of the filter parameters are $\omega_1 = 10$ Hz, $\omega_2 = 5$ Hz, $\omega_3 = 5$ Hz, $\omega_4 = 5$ Hz and $\zeta = 0.7$.

In the DC microgrid, the active power flowing through the VSC is the sum of each of the other units' powers, taking into account a balanced power flow. Hence, when the VSC is forming the DC bus, the power flow can be computed by:

$$P_{vsc} = P_{ess} + P_{dg} + P_{load} + P_{loss} \tag{5}$$

where P_{loss} accounts for all the losses inside the microgrid.

Using the proposed power management strategy, the VSC active power is the only information transmitted from the communication line to the ESS unit, as shown in detail G of Fig. 1. From (5), the power flow inside the microgrid is given essentially by the calculated VSC power, disregarding the internal losses. Therefore, if an autonomous operation is desired, the ESS must provide the calculated VSC power, which corresponds to the mismatch of energy inside the microgrid.

B. Virtual inertia

In a conventional power system, the synchronous generator with its natural inertia of the rotating mass is usually the main source of electrical energy. In a microgrid, however, power electronic converters with very low inertia are the units which establish the bus voltage. Low inertia results in a fast response when transients happen, which makes the whole microgrid vulnerable [37]. In this situation, for autonomous operation of the DC microgrid to occur, the energy storage system must present some inertia to be able to deal with power flow variations and avoid high-rate peaks of power.

As presented in group A of Fig. 1, the proposed PMS starts computing the mismatch, e_p, between the VSC power and the feedback of the ESS power. Hence, $e_p = P_{vsc} - P_{ess}$. The dynamic response of a synchronous machine, as given in (6), can be emulated in order to modify the transient response of the energy storage system [44]:

$$T_m - T_e - D_m\omega = J_m\frac{d\omega}{dt} \tag{6}$$

where T_m and T_e are the mechanical and electromagnetic torque, respectively, D_m is the damping factor, ω is the angular velocity and J_m is the inertia coefficient.

To improve the dynamic response of the ESS, a virtual inertia emulation is added to the PMS, as shown in group A of Fig. 1. The obtained differential equation mimics the behavior given by (6), which leads to:

$$P_{vsc} - P_{ess} - D_p\Delta p = J\left(\frac{d\Delta p}{dt}\right) \tag{7}$$

where J is the inertia coefficient, D_p is the damping coefficient, and Δp is the power mismatch provided or absorbed by the battery bank.

Consequently, the transfer function of the emulated virtual inertia, $K(s)$, is given by:

$$K(s) = \frac{\Delta p}{e_p} = \frac{1}{Js + D_p} \tag{8}$$

The inertia coefficient J is inserted, aiming to enhance the response time of the energy storage system during transients by forcing the VSC to provide the high-rate imbalance of power. This parameter works as a delay by slowing down the ESS response time; choosing this coefficient prevents the ESS from providing undesirable peaks of power inside the DC microgrid. As previously discussed, high-rate current changes may lead to irreversible damage of the battery bank. The damping coefficient, D_p, in its turn, acts as a droop factor, limiting or increasing the power level to be provided or absorbed by the battery bank.

C. ESS management function

A SOC-based function, $\psi\,(soc)$, is applied to manage the ESS charge and discharge process. Since the battery bank is highly utilized in the proposed PMS, the management of the ESS power flow is fundamental to improve the life cycle of the battery bank.

If the power mismatch, Δp, is negative, the ESS enters into the discharging mode. During the discharging mode, the ESS must supply the total power required by the microgrid, i.e. the difference between the power generated by the DG and the power absorbed by the customer load. The ESS should provide the maximum power required by the microgrid until a specified SOC is achieved (soc_a). After this point, the ESS power is linearly reduced until the minimum allowed state of charged is reached (soc_{min}). To avoid an undesirable depth of charge, the battery bank is not allowed to provide any more power after the minimum SOC level is achieved, which means that the AC utility grid must provide the lack of power inside the microgrid. The discharging mode can be computed by (9).

$$\psi\,(soc) = \begin{cases} 0, & SOC \le soc_{\min} \\ \frac{(SOC - soc_{\min})}{(soc_a - soc_{\min})}, & \mathrm{soc}_{\min} < SOC < soc_a \\ 1, & SOC \ge soc_a \end{cases} \tag{9}$$

If the power mismatch is positive, the ESS operates in the charging mode. During the charging mode, the ESS must absorb the surplus of power in the microgrid. The maximum power is absorbed by the battery bank until a specified SOC is achieved (soc_b). After this point, the power going through the ESS is linearly reduced until the maximum allowed state of charge is reached (soc_{max}). To avoid overcharging, the battery bank is not allowed to retain any more power after the maximum SOC level is achieved, hence the surplus of power inside the DC microgrid should flow through the AC utility grid. The charging mode can be computed using (10).

$$\psi\,(soc) = \begin{cases} 1, & SOC \le soc_b \\ 1 - \frac{(SOC - soc_b)}{(soc_{\max} - soc_b)}, & \mathrm{soc}_b < SOC < soc_{\max} \\ 0, & SOC \ge soc_{\max} \end{cases} \tag{10}$$

The choice of the state of charge levels depends upon the topology of the batteries used as energy storage elements. Assuming a generic 50% limit as the depth of discharge, the SOC limits applied in this paper are: $soc_{\max} = 95\%$, $soc_{\min} = 50\%$, $soc_a = 75\%$, $soc_b = 85\%$.

Finally, the ESS reference current for the inner control loop, $I_{ess,ref}$, is obtained by dividing the power mismatch, Δp, between the VSC power, P_{vsc}, and the ESS power, P_{ess}, by the ESS voltage, V_{ess}, considering the virtual inertia emulation, $K(s)$, and the state of charge-based function. The final expression is given by:

$$I_{ess,ref} = e_p \times K(s) \times \psi(soc) \left(\frac{1}{V_{ess}}\right) \tag{11}$$

The energy management system only sees the mismatch between the load requirements and the DG power. If the DG power is not able to attend the load demand, according to the aforementioned strategy, the grid-forming and grid-supporting units must act to keep the power flow balanced.

IV. System Modeling and Controllers Design

A. VSC modeling and control

The control of the voltage source converter is presented in groups D, E, F, and G of Fig. 1. A synchronous reference frame phase-locked loop (SRF-PLL) is used to synchronize the controller with the grid angle, θ_s; thus the dq transformation can be obtained, as shown in group D of Fig. 1. For the VSC working as the grid-forming converter, the dynamics of the DC bus voltage is given by [45]:

$$\frac{C_{bus}}{2}\frac{dV_{bus}^2}{dt} = P_{ext} - P_{loss} - P_t \tag{12}$$

where C_{bus} is the DC bus capacitance, V_{bus} is the DC bus voltage, P_{ext} is an external active power acting as disturbance, P_{loss} is the VSC total losses, and P_t is VSC AC side terminal power. As shown in [45], one can derive:

$$P_t \approx P_s + \left(\frac{2L_{vsc}}{3{V_d}^2}\right)\left(P_s\frac{dP_s}{dt} + Q_s\frac{dQ_s}{dt}\right) \tag{13}$$

where P_s and Q_s are the active and reactive power control inputs, respectively, L_{vsc} is the inductance of the output filter, and V_d is the VSC voltage at the d frame.

Forcing $Q_s = 0$ to achieve unity power factor, the final DC bus dynamics as a function of the controlled active power is given by:

$$\frac{dV_{bus}^2}{dt} = \frac{2}{C_{bus}}\left\{P_{ext} - P_{loss} - \left[P_s + \left(\frac{2L_{vsc}P_s}{3V_d^2}\right)\frac{dP_s}{dt}\right]\right\} \tag{14}$$

As shown in group F of Fig. 1, the dq frame allows a known decoupling between active and reactive power [45]. PI controllers are used to obtain zero steady-state errors for the inner current and outer voltage loops. In order to work with high power factor, the reactive power is set to zero. The dq modulation indexes (m_d, m_q) are obtained from the current controllers and converted back to abc coordinates (m_a, m_b, m_c). Sinusoidal pulse width modulation (SPWM) is applied to activate the IGBTs. The VSC switching frequency, f_{swvsc}, is chosen to achieve low harmonic distortion and fast response.

A simplified control block diagram of the voltage source converter is presented in Fig. 2. The inner current loop control is formed by the PI current controller, $G_{ci}(s)$, by the L filter transfer function, $G_{pi}(s)$, by the PWM transfer function, including its respective delay, $G_d(s)$, and by the sensor feedback transfer function, $H_i(s) = 1$. These functions are given by:

$$G_{pi}(s) = \frac{\tilde{i}_d}{\tilde{d}_{vsc}} = \frac{1}{L_{vsc}s + R_{vsc}} \tag{15}$$

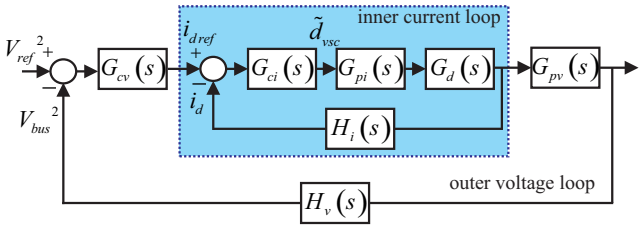

Fig. 2. Control block diagram of the voltage source converter. Each block represents a transfer function described in the text.

$$G_{ci}(s) = \frac{k_{pi}s + k_{ii}}{s} \tag{16}$$

$$G_d(s) = \frac{1}{1 + 1.5T_s s} \tag{17}$$

where L_{vsc} and R_{vsc} are the inductance and equivalent resistance of the output L filter, respectively, k_{pi} and k_{ii} are the proportional and integral gain of the VSC current PI controller, respectively, and $T_s = 10^{-4}$ s is the sampling time.

The outer voltage loop control is formed by the PI voltage controller, $G_{cv}(s)$, by the closed loop transfer function of the inner current control, $G_{cli}(s)$, by the transfer function relating the DC bus voltage and the active power, $G_{pi}(s)$, and by the sensor feedback transfer function, $H_v(s) = 1$. These functions are expressed by:

$$G_{cv}(s) = \frac{k_{pv}s + k_{iv}}{s} \tag{18}$$

$$G_{cli}(s) = \frac{G_{ci}(s)\,G_{pi}(s)\,G_d(s)}{1 + H_i(s)\,G_{ci}(s)\,G_{pi}(s)\,G_d(s)} \tag{19}$$

$$G_{pv}(s) = \frac{\tilde{V}_{bus}^2}{\tilde{P}_{ext}} = \left(\frac{2}{C_{bus}}\right)\left(\frac{\tau_f s + 1}{s}\right) \tag{20}$$

where,

$$\tau_f = \frac{2L_{vsc}P_s}{3{V_d}^2} \tag{21}$$

and k_{pv} and k_{iv} represent the proportional and integral gain of the VSC voltage PI controller, respectively.

The controllers of the VSC were designed by means of a frequency response analysis. To design the PI current controllers, the IGBT switching frequency of 10 kHz (6280 rad/s) was taken into account. Thus, the current loop crossover frequency was set at 4000 rad/s. The controller parameters were designed to achieve a phase margin of 60^o at the crossover frequency. The outer voltage loop was designed to have a much slower dynamic response when compared with the inner current loop control. Hence, the voltage loop crossover frequency was chosen to be 400 rad/s. The controller parameters were designed to achieve a phase margin of 60^o at the crossover frequency. Tab. I displays the values of each converter and control parameters in the DC microgrid.

TABLE I
DC MICROGRID CONVERTERS AND CONTROL PARAMETERS

Circuit	Parameter	Value	Parameter	Value
VSC	P_s (rated)	2.2 kW	ω_0	377 rad/s
	V_d	311 V	V_{bus}	400 V
	L_{vsc}	3.6 mH	R_{vsc}	0.75 Ω
	C_{bus}	4 mF	f_{swvsc}	10 kHz
	k_{pi}	16.7	k_{ii}	663.4
	k_{pv}	0.54	k_{iv}	109.9
Battery	E_{bat}	240 V	Z_B	4 Ω
	L_{ess}	1 mH	C_{ess}	2 mF
	f_{swess}	30 kHz	V_{ess}	220-260 V
	k_{pB}	0.014	k_{iB}	16.67
DG	L_{dg}	1 mH	C_{dg}	2 mF
	f_{swdg}	30 kHz	V_{dg}	127 V
	k_{pd}	0.283	k_{id}	8.151
Load	$P_{load}(rated)$	1 kW	V_{load}	120 V
	L_l	1 mH	C_l	2 mF
	f_{swl}	30 kHz	R_{load}	50 Ω
	k_{pl}	1.316	k_{il}	368.112

B. Energy storage system modeling and control

1) Battery bank model: A battery bank is a cluster of many batteries grouped together in series and/or parallel to achieve the desirable voltage and current rate. The general electric model of a battery bank consists of a dependent DC voltage source in series with an electrical impedance, which represents the battery bank internal voltage and losses, respectively. The state of charge considers the instantaneous amount of charge available in the battery bank. The internal voltage is dependent upon its SOC and the voltage varies as the ESS is absorbing or injecting power [46]. The parameters of each component are chosen based on specific battery technology, such as lead-acid or lithium-ion topologies [47].

Equation (22) describes the behavior of the battery bank model:

$$V_{ess} = E_B(SOC) - Z_B i_{ess} \tag{22}$$

where E_B and V_{ess} are the output and internal battery voltage, respectively, Z_B is the internal impedance and i_{ess} is the battery electrical current. The state of charge can be computed by using the Coulomb counting (ampere-hour balance) method, as given in (23). More precise and sophisticated methods can be consulted in [48], [49].

$$SOC = SOC_0 + \frac{1}{C_{nom}} \int i_{ess} dt \tag{23}$$

where SOC_0 is the initial state of charge and C_{nom} is the battery nominal capacity, usually informed by the manufacturer.

The complexity of the model depends upon which losses one wants to represent. A constant DC source in series with a resistive impedance forms the most common model, for it considers the internal voltage drop and is simple to emulate.

2) ESS control: The energy storage system is composed of a battery bank (discussed in the previous section) connected to the microgrid DC link through a DC-DC bidirectional converter, as presented in Fig. 1. When the utility grid is available, the ESS can be controlled in the current control mode (mode 1 - M1) as a grid-feeding converter. If island operation occurs, the ESS enters on the voltage control mode

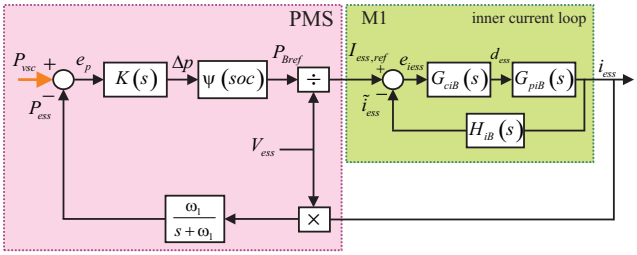

Fig. 3. Control loop of the DC-DC bidirectional converter of the ESS, including the PMS in the grid-connected operation.

(mode 2 - M2), as a grid former, as detailed in group B of Fig. 1. Mode 2 is not covered in this paper. The control loops derived from the small-signal analysis for M1 are presented in Fig. 3.

The control loop of M1 is formed by the PI current controller, $G_{ciB}(s)$, by the transfer function relating current and duty-cycle of the bidirectional DC-DC converter, $G_{piB}(s)$, and by the current sensor transfer function, $H_{iB}(s) = 1$. These functions are expressed by:

$$G_{ciB}(s) = \frac{k_{pB}s + k_{iB}}{s} \tag{24}$$

$$G_{piB}(s) = \frac{\tilde{i}_{ess}}{\tilde{d}_{ess}} = \frac{V_{ess}}{L_{ess}s} \tag{25}$$

where $\tilde{i}_{ess}$ and $\tilde{d}_{ess}$ are the small-signal inductor current, duty-cycle and output voltage, respectively, and L_{ess} is the inductance of the bidirectional DC-DC converter.

If the current control mode is applied, then the reference of power should be given in order to obtain the required inductor current, as discussed in the power management section. The current controller parameters were designed to achieve a phase margin of 60^o at the crossover frequency of 200 rad/s.

C. Distributed generator

The modeling of the distributed generator does not consider any particularities of a topology of generation. If a photovoltaic system or a variable wind turbine is used for the DC microgrid currently under study, the DG system is expected to function by following its respective MPPT algorithms. For the purpose of experiment, the DG emulation is done by using a DC voltage source as a primary source and a boost converter as a link to the DC bus. The boost converter is current controlled using a PI, and its respective modeling is the same presented in (25). The DG parameters are presented in Tab. I. Since the distributed generator is not the aim of the proposed power management strategy, a detailed discussion of the DG controller is omitted in this paper.

D. Customer load converter

The customer load is emulated by a step-down converter regulating the voltage of a resistive load using a PI controller. The load parameters are presented in Tab. I. The relation between the output voltage and the desired duty cycle obtained by the small-signal analysis is given by [50]:

$$G_{vl}(s) = \frac{\tilde{v}_{load}}{\tilde{d}_l} = \frac{V_{bus}}{L_l C_l s^2 + \frac{L_l}{R_{load}} s + 1} \quad (26)$$

where $\tilde{v}_{load}$ and $\tilde{d}_l$ are the small-signal load output voltage and duty cycle, respectively; R_{load} is the load equivalent resistance, and L_l and C_l are the inductance and capacitance of the buck converter, respectively.

V. PMS STABILITY AND PARAMETERS ANALYSIS

A. Stability analysis

The ESS control loop, including the proposed PMS, is shown in Fig. 3. The transfer function $K(s)$ is given in (8); this contains the PMS parameters under analysis, J and D_p. The relation between the power error, e_p, and the ESS reference current, $I_{ess,ref}$, is given by:

$$G_{pms}(s) = \frac{I_{ess,ref}}{e_p} = \left(\frac{1}{V_{ess}}\right) \frac{\psi(soc)}{Js + D_p} \quad (27)$$

By (24) and (25), the closed loop transfer function of the ESS operating in M1 is obtained:

$$G_{cliB}(s) = \frac{i_{ess}}{I_{ess,ref}} = \frac{V_{ess}(k_{pB}s + k_{iB})}{L_{ess}s^2 + V_{ess}(k_{pB}s + k_{iB})} \quad (28)$$

Finally, the feedback of the ESS power is obtained by:

$$H_{pms}(s) = \frac{P_{ess}}{i_{ess}} = V_{ess}\left(\frac{\omega_1}{s + \omega_1}\right) \quad (29)$$

To analyze the influence of the PMS parameters over the ESS control, a stability analysis is conducted. The open loop and closed loop of the energy storage system, including the PMS, are given respectively by:

$$G_{olpms}(s) = \frac{P_{ess}}{e_p} = G_{pms}(s)\, G_{cliB}(s)\, H_{pms}(s) \quad (30)$$

$$G_{clpms}(s) = \frac{i_{ess}}{P_{vsc}} = \frac{G_{pms}(s)\, G_{cliB}(s)}{1 + G_{pms}(s)\, G_{cliB}(s)\, H_{pms}(s)} \quad (31)$$

Substituting (27), (28) and (29) in (30), the final expression for the PMS open loop is:

$$G_{olpms}(s) = \frac{z_0 s + z_1}{p_0 s^4 + p_1 s^3 + p_2 s^2 + p_3 s + p_4} \quad (32)$$

where,

$$\begin{cases} z_0 = \psi V_{ess} \omega_1 K_{pB} \\ z_1 = \psi V_{ess} \omega_1 K_{iB} \\ p_0 = J L_{ess} \\ p_1 = J K_{pB} V_{ess} + (J\omega_1 + D_p) L_{ess} \\ p_2 = J K_{iB} V_{ess} + D_p \omega_1 L_{ess} + (J\omega_1 + D_p) K_{pB} V_{ess} \\ p_3 = D_p \omega_1 K_{pB} V_{ess} + (J\omega_1 + D_p) K_{iB} V_{ess} \\ p_4 = D_p \omega_1 K_{iB} V_{ess} \end{cases}$$

It is assumed that the ESS inner control loop is stable. This condition is fundamental to ensure the correct operation of the power management control. In addition, to simplify the analysis, the battery bank voltage, V_{ess}, is assumed to be constant at 240 V since its variation is limited. The cutoff frequency, ω_1, is part of the low pass filter design with constant value of 5 Hz. The Nyquist plots obtained by varying J and D_p in (32) are presented, respectively, in Figs. 4(a) and 4(b). It is possible to notice that the critical point -1 is not encircled when the parameters J and D_p vary from 0.1 to 10. That means that, for this range of parameters, the stability of the closed loop can only be analyzed by the open loop transfer function according to the Nyquist stability criteria. Thus, for the system to be stable, it is sufficient that the poles of $G_{olpms}(s)$ are kept in the left half-plane.

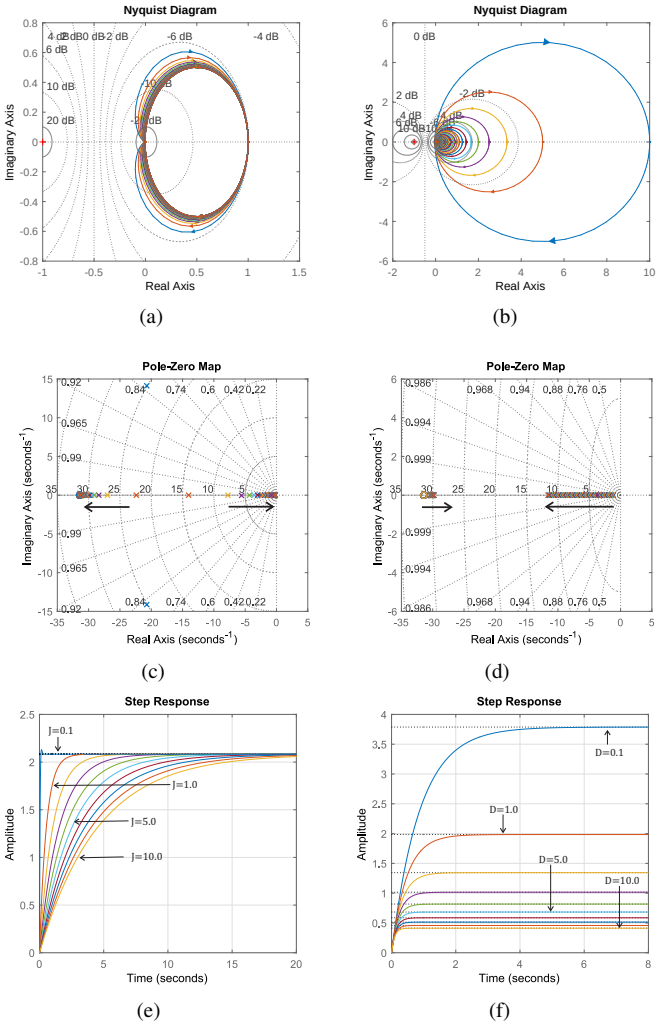

Fig. 4. PMS parameter variation analysis for J and D_p varying from 0.1 to 10. a) Nyquist plot for J variation, b) Nyquist plot for D_p variation, c) Pole-zero mapping for J variation, d) Pole-zero mapping for D_p variation, e) 1 kW step response for J variation, f) 1 kW step response for D_p variation.

The characteristic equation of $G_{olpms}(s)$ derived from (32) is given by:

$$(s + \omega_1)(D_p + Js)\left(L_{ess}s^2 + K_{pB}V_{ess}s + K_{iB}V_{ess}\right) = 0 \quad (33)$$

from where the poles are obtained as:

$$\begin{cases} s_1 = -\omega_1 \\ s_2 = -\frac{D}{J} \\ s_3 = \frac{-K_{pB}V_{ess}}{2L_{ess}} + \sqrt{\left(\frac{K_{pB}V_{ess}}{2L_{ess}}\right)^2 - \frac{K_{iB}V_{ess}}{L_{ess}}} \\ s_4 = \frac{-K_{pB}V_{ess}}{2L_{ess}} - \sqrt{\left(\frac{K_{pB}V_{ess}}{2L_{ess}}\right)^2 - \frac{K_{iB}V_{ess}}{L_{ess}}} \end{cases} \quad (34)$$

From s_3 and s_4, since K_{piB}, V_{ess} and L_{ess} are positive values, it is possible to conclude that these parameters are not able to destabilize the system. It is important, however, that a correct design of the PI current control is followed. From s_1, it is observed that the choice of the cutoff frequency of the LPF, ω_1, does affect the system behavior, although ω_1 positive is enough to prevent this pole from crossing to the right half-plane. A small value of ω_1 forces this pole to approach the origin. Finally, from s_2 analysis, it is clear that the PMS parameters must assume positive and not null values in order to achieve stability.

The mapping of poles and zeros of the closed loop transfer function, $G_{clpms}(s)$, when J and D_p increases, are presented in Figs. 4(c) and 4(d), respectively. The arrows indicate the march of the dominant poles when the parameters increase. Assuming J and D_p are positive and not null is sufficient to avoid instability. However, the increasing of J values forces the dominant poles of $G_{clpms}(s)$ to approach the origin, which leads to an undesired stability margin. On the other hand, the increasing of D_p values makes the dominant poles move away from the origin. Hence, a tradeoff between the factor D_p/J has to be done to achieve the desired system behavior.

B. Parameter analysis

A step of power is applied over $G_{clpms}(s)$ to obtain the current when the rated power is required ($P_{ess} = 1$ kW). From Fig. 4(e) it becomes clear that the parameter J affects the system time response, changing the inertia of the ESS. A low value of J makes the response fast, while larger values reduce the response time. From Fig. 4(f), for a fixed value of J, changing the parameter D_p results in a steady-state error. A value of D_p inferior to 1 leads to a steady-state value larger than the expected, while a value superior to 1 leads to a smaller steady-state response. Hence, D_p equals to 1 is the choice applied in this paper. To summarize:

- The inner current loop control must be stable for the PMS to operate correctly; this is achieved by a proper design of the PI compensator parameters, K_{piB} and K_{iiB}.
- Low values of the LPF cutoff frequency, ω_1, leads the system into marginal stability. Thus, these values must be taken into account when designing the filter.
- Parameters J and D_p must be positive and not null. Values closed to zero are not allowed, in order to avoid a small stability margin in the system. Higher values of J degrade the stability margin, while higher values of D_p contributes to it. Therefore, a tradeoff for D_p/J must be considered.
- Finally, the parameter J affects the ESS time response, while D_p affects the steady-state response. Higher values of J increase the system time response. Higher values of D_p lead to a smaller steady-state value. To achieve the expected steady-state value, $D_p = 1$ is used.

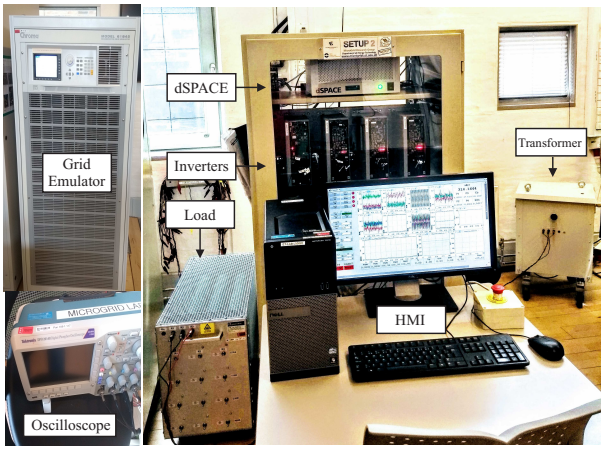

Fig. 5. Experimental setup formed by 4 inverters, voltage and current sensors, data acquisition, a dSPACE, human-machine interface, set of resistive loads, grid emulator, isolation transformer, and an oscilloscope.

VI. Experimental Results

A. Experimental Setup

The experimental setup shown in Fig. 5 is formed by four *Danfoss FC302* inverters, a *dSPACE DS1006* processor board as a central controller, an AC grid emulator *Chroma 61845*, a set of resistive loads, and an isolation transformer *Dyn11*; the latter was used to isolate the microgrid converters from the utility grid in the laboratory. *LEM* current and voltage sensors were used to obtain the desired signals and the acquisition boards *DS2004* linked the sensors to the *dSPACE*. A human-machine interface (HMI) was utilized to collect the data and run the experiments. The images presented in this section were collected by using an oscilloscope *Tektronix DPO 2014B*. The ESS, including the battery bank model and the bidirectional DC-DC converter, was emulated in the *dSPACE* using the AC grid as the source of power and the *Danfoss* inverter as the power electronic converter.

The objective of the power flow presented in Fig. 6(a) is to submit the DC microgrid to critical conditions. A positive value indicates that the power is being absorbed, while a negative value indicates that power is being supplied by the source. The total experiment time was 200 s. In Fig. 6(a), at the moment $T_1 = 20$ s, the maximum load power is required inside the microgrid and the DG does not contribute to the power flow. This test is applied to verify the behavior of the DC microgrid with the proposed PMS when the ESS is the only source of power. At the instant $T_2 = 100$ s, the DG power is increased in ramp until its rated power is achieved. Between T_1 and T_2, the load power and DG power flow into the system. After $T_3 = 120$ s, the loads are cut off to emulate a critical situation in which the DG still provides power, but no load is present to consume this extra energy. The aforementioned presets do not change for the following experimental runs.

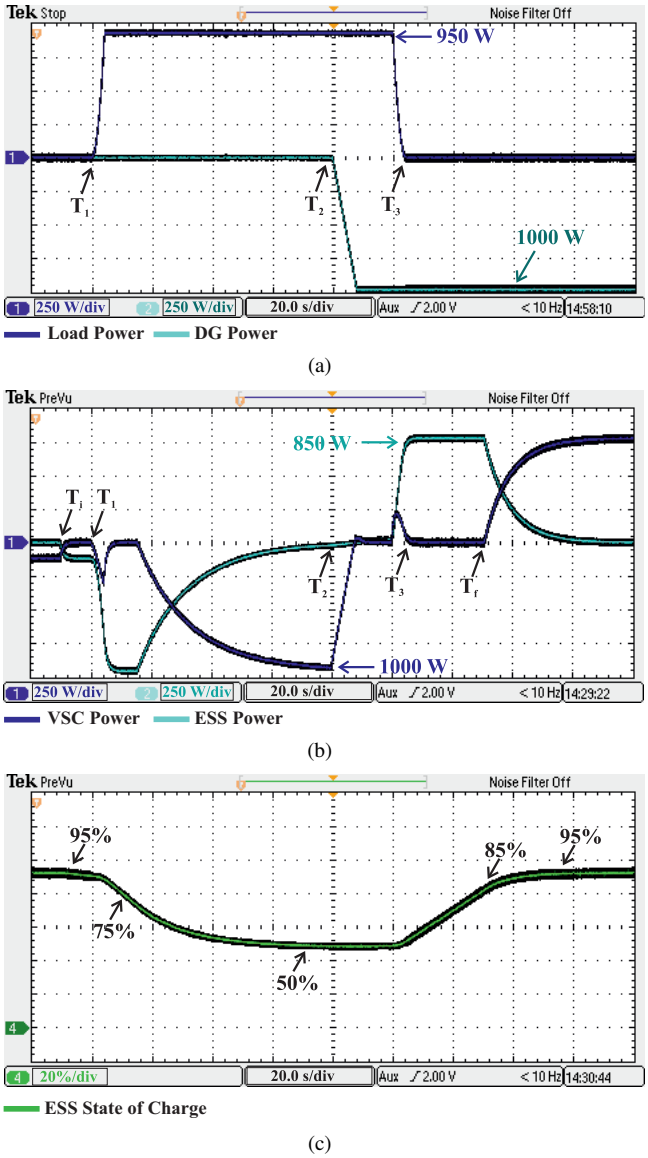

Fig. 6. Experimental results showing the power flow inside the DC microgrid. a) In dark blue: load power consumption. In light blue: DG power supply; b) In dark blue: VSC power. In light blue: ESS power for $J = 1.0$, $D_p = 1.0$; c) Estimated ESS state of charge.

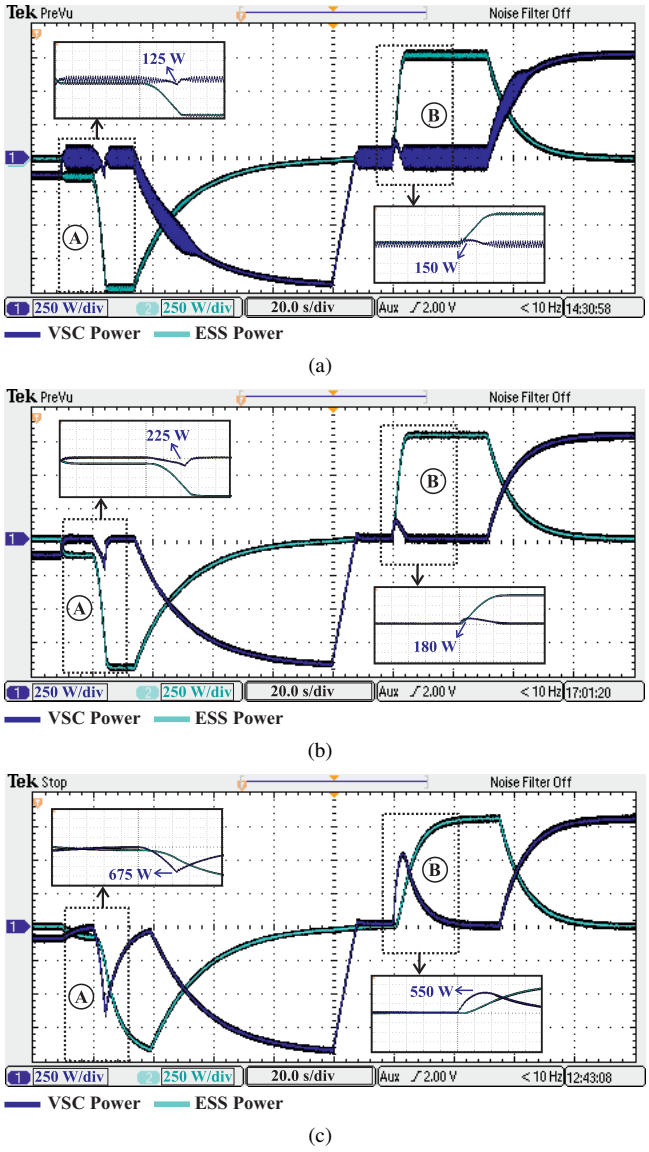

Fig. 7. Experimental results showing the power flow inside the DC microgrid when the parameter J is changed. In dark blue: VSC power. In light blue: ESS power a) $J = 0.1$; b) $J = 0.5$; c) $J = 5.0$.

B. Power flow and SOC management analysis

To allow experimental tests in a reasonable time and amount of data, and considering the level of power in the experiments, the emulated battery bank had its nominal capacity designed to be fully charged and discharged in approximately 10 minutes. Thus, the PMS parameters were adjusted for this situation. In a real system, it would take hours to charge and discharge the battery bank, which is not practical for study purposes. For the load and DG preset power flow shown in Fig. 6(a), the behavior of the ESS and utility grid using the proposed PMS is presented in Fig. 6(b). For fixed parameters $J = 1$ and $D_p = 1$, the effect of the power flow and the SOC management function is evaluated. The battery bank state of charge during the test is depicted in Fig. 6(c), in which the initial SOC was set to 95 %.

From Fig. 6(b), it is possible to observe that before the instant T_i, the AC utility grid is responsible for providing the power losses in the DC microgrid ($\approx$ 100 W). At $T_i = 10$ s, the PMS is activated and the ESS becomes responsible for supplying the power required in the system. At T_1, the loads start to consume the rated power of 950 W. After the transient, the ESS starts to provide the required power, which is maintained until the state of charge limit of 75 % is achieved. At this moment, the SOC management function forces the battery bank to smoothly provide less power until the minimum SOC of 50 % is reached and, henceforward, the ESS stops providing power. During this period, the VSC provides the power to fill the lack inside the microgrid. At the instant T_2, the DG starts to inject power into the system, reducing the power provided by the VSC, while the ESS power is kept null. When T_3 is reached, the loads are cut off. As a result of the PMS operation, the battery bank starts to absorb the surplus of power. When the SOC level of 85 % is reached,

the ESS smoothly reduces the absorbed power, which in time starts to flow through the AC utility grid. When the maximum SOC level of 95 % is achieved at $T_f = 150$ s, the ESS stops absorbing the extra energy, and all the power generated by the DG goes through the AC grid.

C. Virtual inertia analysis

The effect of changing the ESS inertia is observed in Figs. 7(a), 7(b) and 7(c). The transients of power, highlighted in the details A and B, are affected by the inertia value. The peak of power during the transient is displayed in each detail cut. For $J = 0.1$, the system presents undesired power oscillations, confirming what was mentioned previously: the inertia parameters should not be close to zero. When parameter J increases, the ESS inertia is augmented, which leads to a higher instantaneous peak of power provided by the VSC. The control over the transient power is important for protecting the ESS against high peaks of current and to avoid instability inside the microgrid. However, a high inertia degrades the ability of the ESS to supply or absorb the required power, as can be seen when the inertia parameter is increased to $J = 5.0$. Changing the inertia parameter does not affect the ESS management function, and the limits of the battery bank state of charge are maintained. For this experimental test, the choice $J = 1.0$ leads to a good tradeoff between transient response limitation and adequate time to achieve the steady-state response.

Figs. 8(a), 8(b), 8(c), and 8(d) display the effect of changing the parameter J over the DC bus voltage. The voltage peak and the main instants of consideration are marked. Only the voltage variation was captured to allow a better visualization; thus, the 400 V level was used as the ground reference. It is possible to infer that even very low inertia ($J = 0.1$) does not destabilize the DC voltage inside the microgrid. The VSC voltage control is responsible for keeping the level and stability of the DC bus voltage. However, since the PMS with low inertia parameter drives the ESS system to marginal stability, this behavior is reflected on the DC voltage oscillations, which is not desirable. For all the presented cases, voltage transient variations were observed when the load or DG power increases. This behavior is associated with the VSC dynamic response and barely affected by the PMS operation. When a proper inertia value is selected, the maximum observed voltage variation was approximately 6 V for $J = 5.0$. Hence, one can conclude that for the DC microgrid operating in the grid-connected mode, the proposed power management strategy with the proper parameter design does not significantly affect the DC bus voltage transient response.

The final observation to be made is the effect of changing the damping parameter D_p for the selected inertia value $J = 1$. This effect can be seen in Figs. 9(a) and 9(b) . For $D_p = 0.5$, the PMS forces the ESS to provide more power than required by the DC microgrid whenever the loads are on. As a result, the ESS injects power into the AC grid. Conversely, when the DG injects surplus power, the PMS forces the ESS to absorb more power than the DC microgrid is able to supply. Therefore, the VSC starts to provide power to the ESS. For

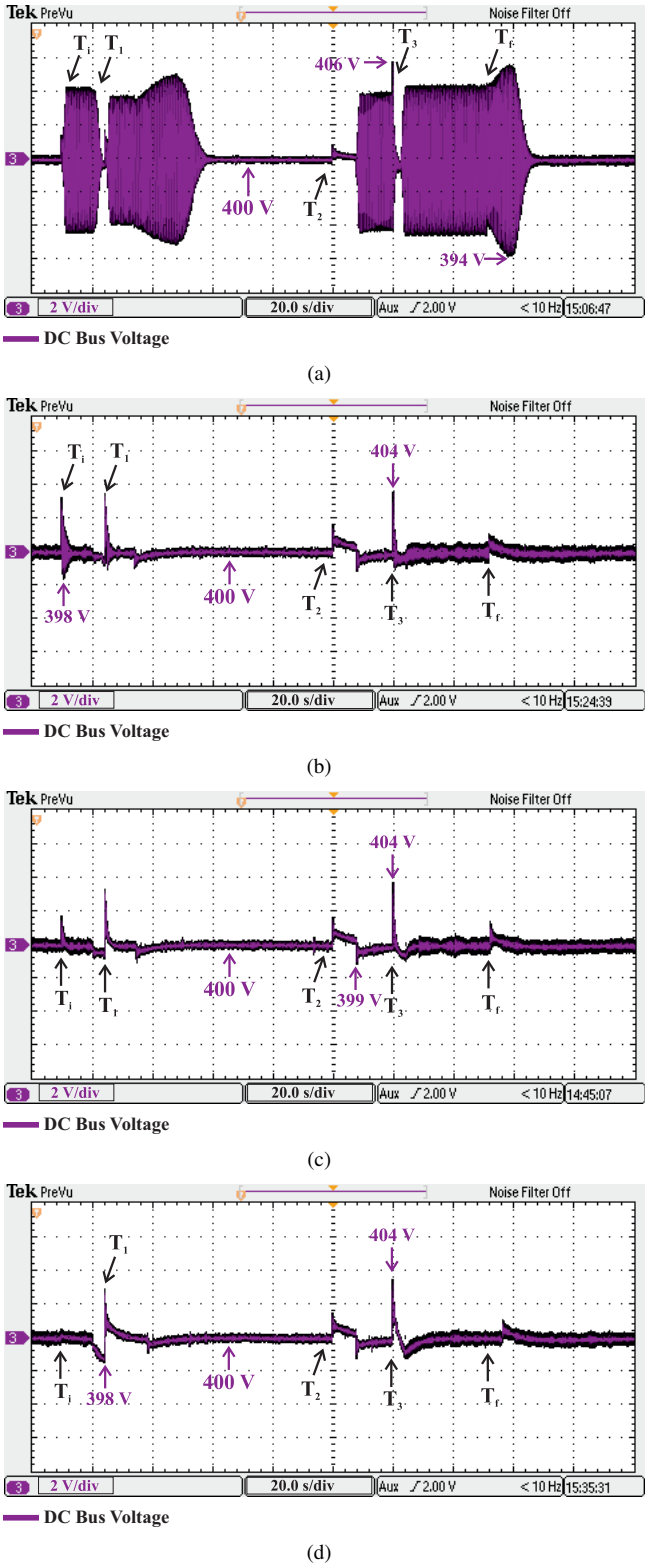

Fig. 8. Experimental results containing the DC bus voltage of the DC microgrid when the inertia parameter J is changed. a) $J = 0.1$; b) $J = 0.5$; c) $J = 1.0$; d) $J = 5.0$.

$D_p = 2.0$, the ESS and VSC share the same amount of power injected or absorbed until the ESS state of charge limitations are achieved. Although, for this study, the choice for $D_p = 1.0$ is the right selection, it is observed that this parameter gives

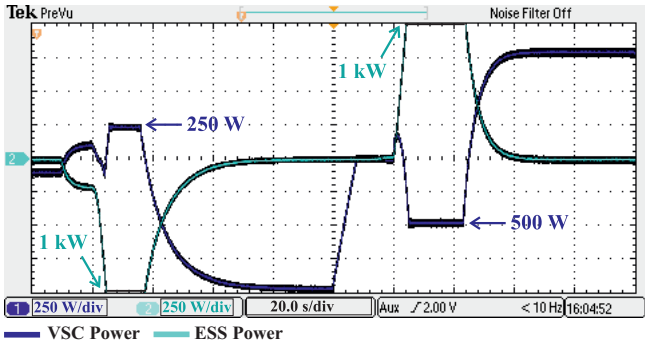

(a)

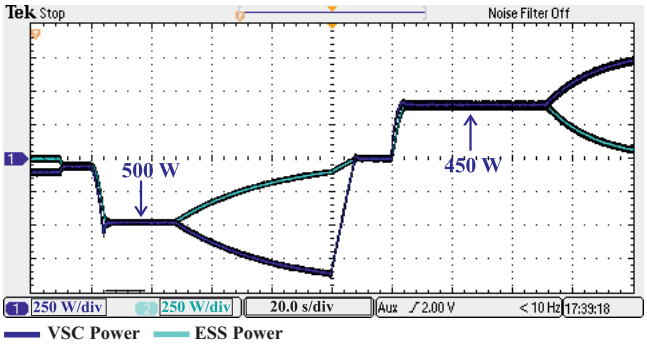

(b)

Fig. 9. Experimental results containing the effect of changing parameter D_p. In dark blue: VSC power. In light blue: ESS power. a) $D_p = 0.5$; b) $D_p = 2.0$.

an extra degree of freedom in controlling the ESS. This extra degree of freedom can be applied to the power sharing of parallel units and price fluctuation in the energy market, which will be considered in further studies.

VII. Conclusion

This paper has presented a power management strategy for DC microgrids operating in the grid-connected mode. The proposed power management system relies on a communication link between converters; however, the AC grid active power is the only information required to be transmitted to the energy storage system, which simplifies the communication link. Autonomous operation is achieved inside the DC microgrid, with the AC utility grid only providing the surplus or shortage of power when the ESS is not capable of injecting or absorbing more energy due to state of charge limitations.

A virtual inertia technique was applied to control the ESS transient response by increasing the inertia of the system. The choice of the virtual inertia parameters was properly addressed in the paper. A state of charge-based management function was used to limit the ESS operation in safe levels, avoiding the depth and overcharge of the battery bank; this function contributes to improving the battery bank life cycle. It was verified that a proper selection of the PMS parameters increases the microgrid performance without deteriorating the DC link bus voltage. The experimental results show that the proposed PMS is reliable, leading the system to autonomous operation and a smooth power flow inside the DC microgrid. Finally, the proposed PMS introduces an extra degree of freedom of control over the energy storage system, which can be explored in further research.

References

[1] J. J. Justo, F. Mwasilu, J. Lee, and J. W. Jung, "AC-microgrids versus DC-microgrids with distributed energy resources: A review," *Renewable and Sustainable Energy Reviews*, vol. 24, pp. 387–405, 2013.

[2] D. Kumar, F. Zare, and A. Ghosh, "DC Microgrid Technology: System Architectures, AC Grid Interfaces, Grounding Schemes, Power Quality, Communication Networks, Applications and Standardizations Aspects," *IEEE Access*, vol. 5, pp. 1–1, 2017.

[3] L. Meng, Q. Shafiee, G. Ferrari Trecate, H. Karimi, D. Fulwani, X. Lu, and J. M. Guerrero, "Review on Control of DC Microgrids," *IEEE Journal of Emerging and Selected Topics in Power Electronics*, vol. 5, no. 3, pp. 1–1, 2017.

[4] E. Cetin, A. Yilanci, H. K. Ozturk, M. Colak, I. Kasikci, and S. Iplikci, "A micro-DC power distribution system for a residential application energized by photovoltaic-wind/fuel cell hybrid energy systems," *Energy and Buildings*, vol. 42, no. 8, pp. 1344–1352, 2010.

[5] B. Liu, F. Zhuo, Y. Zhu, and H. Yi, "System Operation and Energy Management of a Renewable Energy-Based DC Micro-Grid for High Penetration Depth Application," *IEEE Transactions on Smart Grid*, vol. 6, no. 3, pp. 1147–1155, 2015.

[6] A. Iovine, S. B. Siad, G. Damm, E. De Santis, and M. D. Di Benedetto, "Nonlinear Control of a DC MicroGrid for the Integration of Photovoltaic Panels," *IEEE Transactions on Automation Science and Engineering*, vol. 14, no. 2, pp. 524–535, 2017.

[7] F. Cingoz, A. Elrayyah, and Y. Sozer, "Optimized Settings of Droop Parameters Using Stochastic Load Modeling for Effective DC Microgrids Operation," *IEEE Transactions on Industry Applications*, vol. 53, no. 2, pp. 1358–1371, 2017.

[8] X. Li, L. Guo, S. Zhang, C. Wang, Y. W. Li, A. Chen, and Y. Feng, "Observer-Based DC Voltage Droop and Current Feed-Forward Control of a DC Microgrid," *IEEE Transactions on Smart Grid*, vol. 9, no. 5, pp. 5207–5216, 2018.

[9] T. Dragicevic, X. Lu, J. Vasquez, and J. Guerrero, "DC Microgrids—Part I: A Review of Control Strategies and Stabilization Techniques," *IEEE Transactions on Power Electronics*, vol. 8993, no. c, pp. 1–1, 2015.

[10] P. H. Huang, P. C. Liu, W. Xiao, and M. S. El Moursi, "A Novel Droop-Based Average Voltage Sharing Control Strategy for DC Microgrids," *IEEE Transactions on Smart Grid*, vol. 6, no. 3, pp. 1096–1106, 2015.

[11] J. M. Guerrero, J. C. Vasquez, J. Matas, L. G. De Vicuña, and M. Castilla, "Hierarchical control of droop-controlled AC and DC microgrids - A general approach toward standardization," *IEEE Transactions on Industrial Electronics*, vol. 58, no. 1, pp. 158–172, 2011.

[12] C. Jin, P. Wang, J. Xiao, Y. Tang, and F. H. Choo, "Implementation of Hierarchical Control in DC Microgrids," *IEEE Transactions on Industrial Electronics*, vol. 61, no. 8, pp. 4032–4042, aug 2014.

[13] T. R. Oliveira, W. W. A. Gonçalves Silva, and P. F. Donoso-Garcia, "Distributed secondary level control for energy storage management in DC microgrids," *IEEE Transactions on Smart Grid*, vol. 8, no. 6, pp. 2597–2607, 2017.

[14] T. Dragicevi, J. M.Guerrero, and J. C. C. Vasquez, "A Distributed Control Strategy for Coordination of an Autonomous LVDC Microgrid Based onPower-Line Signaling," *IEEE Transactions on Industrial Electronics*, vol. 61, no. 7, pp. 3313–3326, 2014.

[15] T. Morstyn, B. Hredzak, G. Demetriades, and V. Agelidis, "Unified Distributed Control for DC Microgrid Operating Modes," *IEEE Transactions on Power Systems*, vol. PP, no. PP, pp. 1–11, 2015.

[16] V. Nasirian, S. Moayedi, A. Davoudi, and F. L. Lewis, "Distributed Cooperative Control of DC Microgrids," *IEEE Transactions on Power Electronics*, vol. 30, no. 4, pp. 2288–2303, 2015.

[17] J. Zhao and F. Dörfler, "Distributed control and optimization in DC microgrids," *Automatica*, vol. 61, pp. 18–26, 2015.

[18] G. Ferrari-Trecate, J. C. Vasquez, M. Tucci, S. Riverso, and J. M. Guerrero, "A Decentralized Scalable Approach to Voltage Control of DC Islanded Microgrids," *IEEE Transactions on Control Systems Technology*, vol. 24, no. 6, pp. 1965–1979, 2016.

[19] V. Nasirian, S. S. Member, A. Davoudi, F. L. Lewis, J. M. Guerrero, and S. S. Member, "Distributed Adaptive Droop Control for DC Distribution Systems," *IEEE Transactions on Energy Conversion*, vol. 29, no. 4, pp. 944–956, 2014.

[20] X. Lu, K. Sun, J. M. Guerrero, J. C. Vasquez, and L. Huang, "Double-Quadrant State-of-Charge Based Droop Control Method for Distributed Energy Storage Systems in Autonomous DC Microgrids," *IEEE Transactions on Smart Grid*, vol. 6, no. 1, pp. 147 – 157, 2015.

[21] J. Xiao, L. Setyawan, P. Wang, and C. Jin, "Power-Capacity-Based Bus-Voltage Region Partition and Online Droop Coefficient Tuning for Real-Time Operation of DC Microgrids," *IEEE Transactions on Energy Conversion*, vol. 30, no. 4, pp. 1338–1347, 2015.

[22] M. Hamzeh, M. Ghafouri, H. Karimi, K. Sheshyekani, and J. M. Guerrero, "Power Oscillations Damping in DC Microgrids," *IEEE Transactions on Energy Conversion*, vol. 31, no. 3, pp. 970–980, 2016.

[23] X. Hou, Y. Sun, Z. Liu, H. Han, and M. Su, "Stability Analysis and Stabilization Methods of DC Microgrid With Multiple Parallel-Connected DC–DC Converters Loaded by CPLs," *IEEE Transactions on Smart Grid*, vol. 9, no. 1, pp. 132–142, 2016.

[24] L. Herrera, W. Zhang, and J. Wang, "Stability Analysis and Controller Design of DC Microgrids with Constant Power Loads," *IEEE Transactions on Smart Grid*, vol. 8, no. 2, pp. 881–888, 2017.

[25] A. M. Gee, F. V. Robinson, and R. W. Dunn, "Analysis of battery lifetime extension in a small-scale wind-energy system using supercapacitors," *IEEE Transactions on Energy Conversion*, vol. 28, no. 1, pp. 24–33, 2013.

[26] H. Samani and X. Fernando, "Battery Current's Fluctuations Removal in Hybrid Energy Storage System Based on Optimized Control of Supercapacitor Voltage," *IEEE Embedded Systems Letters*, vol. 8, no. 3, pp. 53–56, 2016.

[27] A. Hosseinipour and H. Hojabri, "Virtual inertia control of PV systems for dynamic performance and damping enhancement of DC microgrids with constant power loads," *IET Renewable Power Generation*, vol. 12, no. 4, pp. 430–438, 2018.

[28] N. Kularatna, "Rechargeable batteries and their management: Part 30 in a series of tutorials on instrumentation and measurement," *IEEE Instrumentation and Measurement Magazine*, vol. 14, no. 2, pp. 20–33, 2011.

[29] M. A. Hannan, M. M. Hoque, A. Hussain, Y. Yusof, and P. J. Ker, "State-of-the-Art and Energy Management System of Lithium-Ion Batteries in Electric Vehicle Applications: Issues and Recommendations," *IEEE Access*, vol. 6, pp. 19 362–19 378, 2018.

[30] A. Khaligh and Z. Li, "Battery, ultracapacitor, fuel cell, and hybrid energy storage systems for electric, hybrid electric, fuel cell, and plug-in hybrid electric vehicles: State of the art," *IEEE Transactions on Vehicular Technology*, vol. 59, no. 6, pp. 2806–2814, 2010.

[31] S. Vazquez, S. M. Lukic, E. Galvan, L. G. Franquelo, and J. M. Carrasco, "Energy storage systems for transport and grid applications," *IEEE Transactions on Industrial Electronics*, vol. 57, no. 12, pp. 3881–3895, 2010.

[32] H. Zhou, T. Bhattacharya, D. Tran, T. S. T. Siew, and A. M. Khambadkone, "Composite energy storage system involving battery and ultracapacitor with dynamic energy management in microgrid applications," *IEEE Transactions on Power Electronics*, vol. 26, no. 3, pp. 923–930, 2011.

[33] R. H. Byrne, T. A. Nguyen, D. A. Copp, B. R. Chalamala, and I. Gyuk, "Energy Management and Optimization Methods for Grid Energy Storage Systems," *IEEE Access*, vol. 6, pp. 13 231–13 260, 2017.

[34] J. Fang, Y. Tang, H. Li, and X. Li, "A Battery/Ultracapacitor Hybrid Energy Storage System for Implementing the Power Management of Virtual Synchronous Generators," *IEEE Transactions on Power Electronics*, vol. 33, no. 4, pp. 2820–2824, 2018.

[35] D. Wu, F. Tang, T. Dragicevic, J. M. Guerrero, and J. C. Vasquez, "Coordinated control based on bus-signaling and virtual inertia for Islanded DC Microgrids," *IEEE Transactions on Smart Grid*, vol. 6, no. 6, pp. 2627–2638, 2015.

[36] D. Chen, Y. Xu, and A. Q. Huang, "Integration of DC Microgrids as Virtual Synchronous Machines into the AC Grid," *IEEE Transactions on Industrial Electronics*, vol. 64, no. 9, pp. 7455–7466, 2017.

[37] W. Wu, Y. Chen, A. Luo, L. Zhou, X. Zhou, L. Yang, Y. Dong, and J. M. Guerrero, "A Virtual Inertia Control Strategy for DC Microgrids Analogized with Virtual Synchronous Machines," *IEEE Transactions on Industrial Electronics*, vol. 64, no. 7, pp. 6005–6016, 2017.

[38] S. Samanta, J. P. Mishra, and B. K. Roy, "Virtual DC machine: An inertia emulation and control technique for a bidirectional DC-DC converter in a DC microgrid," *IET Electric Power Applications*, vol. 12, no. 6, pp. 874–884, 2018.

[39] K. Shi, H. Ye, W. Song, and G. Zhou, "Virtual Inertia Control Strategy in Microgrid Based on Virtual Synchronous Generator Technology," *IEEE Access*, vol. 6, pp. 27 949–27 957, 2018.

[40] S. Samanta, J. Mishra, and B. Roy, "AC Load Bus Frequency Control of a DC Microgrid based on DC Voltage Regulation using Inertia Emulation and Economic Power Management," *IET Generation, Transmission & Distribution*, vol. 13, pp. 5117–5128, 2019.

[41] Z. Yi, X. Zhao, D. Shi, J. Duan, Y. Xiang, and Z. Wang, "Accurate Power Sharing and Synthetic Inertia Control for DC Building Microgrids with Guaranteed Performance," *IEEE Access*, vol. 7, pp. 63 698–63 708, 2019.

[42] M. Saleh, Y. Esa, and A. Mohamed, "Impact of communication latency on the bus voltage of centrally controlled dc microgrids during islanding," *IEEE Transactions on Sustainable Energy*, vol. 10, no. 4, pp. 1844–1856, Oct 2019.

[43] M. Saleh, Y. Esa, and A. A. Mohamed, "Communication-Based Control for DC Microgrids," *IEEE Transactions on Smart Grid*, vol. 10, no. 2, pp. 2180–2195, 2019.

[44] Q. C. Zhong and G. Weiss, "Synchronverters: Inverters that mimic synchronous generators," *IEEE Transactions on Industrial Electronics*, vol. 58, no. 4, pp. 1259–1267, 2011.

[45] A. Yazdani and R. Iravani, *Voltage-Sourced Converters in Power Systems: Modeling, Control, and Applications*, ser. Wiley - IEEE. Wiley, 2010.

[46] M. Coleman, C. K. Lee, C. Zhu, and W. G. Hurley, "State-of-charge determination from EMF voltage estimation: Using impedance, terminal voltage, and current for lead-acid and lithium-ion batteries," *IEEE Transactions on Industrial Electronics*, vol. 54, no. 5, pp. 2550–2557, 2007.

[47] S. Barsali and M. Ceraolo, "Dynamical models of lead-acid batteries: Implementation issues," *IEEE Transactions on Energy Conversion*, vol. 17, no. 1, pp. 16–23, 2002.

[48] M. A. Hannan, M. S. Lipu, A. Hussain, and A. Mohamed, "A review of lithium-ion battery state of charge estimation and management system in electric vehicle applications: Challenges and recommendations," *Renewable and Sustainable Energy Reviews*, vol. 78, no. May, pp. 834–854, 2017.

[49] R. Xiong, J. Cao, Q. Yu, H. He, and F. Sun, "Critical Review on the Battery State of Charge Estimation Methods for Electric Vehicles," *IEEE Access*, vol. 6, pp. 1832–1843, 2017.

[50] F. Blaabjerg, *Control of Power Electronic Converters and Systems*. Elsevier Science, 2018, no. v. 1.

Pedro José dos Santos Neto (S'16) received the B.S. degree in electrical engineering in 2016 from the Federal University of Vale do São Francisco (UNIVASF), Petrolina, Brazil, and the M.S. degree in 2017 from the University of Campinas (UNICAMP), Campinas, Brazil. He is currently pursuing his Ph.D. degree from UNICAMP, at the Power Electronics Lab (LEPO), under the São Paulo Research Foundation (FAPESP) scholarship program. In 2019, he was a Guest Ph.D. visitor with the Center for Research on Microgrids (CROM) at the Aalborg University, Aalborg East, Denmark. He works in the areas of microgrids, electrical machines, and power electronics. His research interests include DC microgrids, renewable energy, and switched reluctance machines. He is a student member of the IEEE and the Brazilian Society of Power Electronics (SOBRAEP).

Tárcio André dos Santos Barros (S'14–M'17) received the B.S. degree in electrical engineering in 2010 from the Federal University of Vale do São Francisco (UNIVASF), Petrolina, Brazil, and M.S. and Ph.D. degrees from the University of Campinas (UNICAMP), Campinas, Brazil, in 2012 and 2015, respectively. From 2016 to 2017, he was a researcher with the University of Campinas, at the Power Electronics Lab (LEPO), under the FAPESP Postdoctoral Program. He is currently a Professor with the Mechanical Engineering Faculty, UNICAMP, and a Coordinating Member of the Brazilian government program ROTA 2030 (electric vehicles). He works in the areas of electrical machines, power electronics, electrical vehicles, and electrical drives. His research interests include machine drives, switched reluctance machines, doubly fed induction generators, and solar energy. He is a member of the IEEE, PELS and Brazilian Society of Power Electronics (SOBRAEP).

João Pedro Carvalho Silveira (S'20) receive the B.S. degree in energy engineering, in 2013, and M.S. degree in electrical engineering, in 2016, both from the University of Brasilia (UnB), Brasilia, Brazil. He is currently working toward the Ph.D. degree with the University of Campinas, Campinas, Brazil, at the Power Electronics Lab (LEPO), under the CAPES scholarship program. He works in the areas of electrical machines, power electronics, and electrical drives. His research interests include microgrids, energy storage systems, renewable energy, distributed generation and power quality.

Ernesto Ruppert Filho (M'00) received the B.S. degree in electrical engineering and the M.S. and Ph.D. degrees from the University of Campinas (UNICAMP), Campinas, Brazil, in 1971, 1974, and 1983, respectively. From 1972 to 1978, he was with the Electrical and Computer Engineering School, UNICAMP, as an Assistant Professor of electromechanical energy conversion. From 1979 to 1983, he was with General Electric, Brazil, designing large induction and synchronous motors and working as an Application Engineer dedicated to large motors and generators. From 1983 to 1989, he was with Vigesa Heavy Equipment, Brazil, designing very large hydrogenerators and also performing commissioning tests on hydropower plants in Brazil. Founder of the Power Electronics Lab (LEPO), UNICAMP. He is currently a Full Professor with the Electrical and Computer Engineering School, UNICAMP, researching and teaching in the areas of electrical machines, power electronics, drives, and electrical power systems.

Juan C. Vasquez (M'12-SM'14) received the B.S. degree in electronics engineering from the Autonomous University of Manizales, Manizales, Colombia, and the Ph.D. degree in automatic control, robotics, and computer vision from BarcelonaTech-UPC, Spain, in 2004 and 2009, respectively. In 2011, He was Assistant Professor and in 2014, Associate Professor at the Department of Energy Technology, Aalborg University, Denmark. In 2019, He became Professor in Energy Internet and Microgrids and currently He is the Co-Director of the Villum Center for Research on Microgrids (see crom.et.aau.dk). He was a Visiting Scholar at the Center of Power Electronics Systems (CPES) at Virginia Tech, USA and a visiting professor at Ritsumeikan University, Japan. His current research interests include operation, advanced hierarchical and cooperative control, optimization and energy management applied to distributed generation in AC/DC Microgrids, maritime microgrids, advanced metering infrastructures and the integration of Internet of Things and Energy Internet into the SmartGrid. Prof.Vasquez is an Associate Editor of IET POWER ELECTRONICS and a Guest Editor of the IEEE TRANSACTIONS ON INDUSTRIAL INFORMATICS Special Issue on Energy Internet. Prof. Vasquez was awarded as Highly Cited Researcher by Thomson Reuters from 2017 to 2019 and He was the recipient of the Young Investigator Award 2019. He has published more than 450 journal papers in the field of Microgrids, which in total are cited more than 19000 times. Dr. Vasquez is currently a member of the IEC System Evaluation Group SEG4 on LVDC Distribution and Safety for use in Developed and Developing Economies, the Renewable Energy Systems Technical Committee TC-RES in IEEE Industrial Electronics, PELS, IAS, and PES Societies.

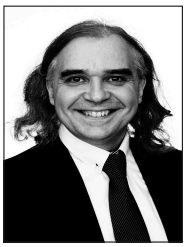

Josep M. Guerrero (S'01-M'04-SM'08-FM'15) received the B.S. degree in telecommunications engineering, the M.S. degree in electronics engineering, and the Ph.D. degree in power electronics from the Technical University of Catalonia, Barcelona, in 1997, 2000 and 2003, respectively. Since 2011, he has been a Full Professor with the Department of Energy Technology, Aalborg University, Denmark, where he is responsible for the Microgrid Research Program. From 2014 he is chair Professor in Shandong University; from 2015 he is a distinguished guest Professor in Hunan University; and from 2016 he is a visiting professor fellow at Aston University, UK, and a guest Professor at the Nanjing University of Posts and Telecommunications. From 2019, he became a Villum Investigator by The Villum Fonden, which supports the Center for Research on Microgrids (CROM) at Aalborg University, being Prof. Guerrero the founder and Director of the same centre (www.crom.et.aau.dk). His research interests is oriented to different microgrid aspects, including power electronics, distributed energy-storage systems, hierarchical and cooperative control, energy management systems, smart metering and the internet of things for AC/DC microgrid clusters and islanded minigrids. Specially focused on microgrid technologies applied to offshore wind and maritime microgrids for electrical ships, vessels, ferries and seaports. Prof. Guerrero is an Associate Editor for a number of IEEE TRANSACTIONS. He has published more than 500 journal papers in the fields of microgrids and renewable energy systems, which are cited more than 50,000 times. He received the best paper award of the IEEE Transactions on Energy Conversion for the period 2014-2015, and the best paper prize of IEEE-PES in 2015. As well, he received the best paper award of the Journal of Power Electronics in 2016. During six consecutive years, from 2014 to 2019, he was awarded by Clarivate Analytics (former Thomson Reuters) as Highly Cited Researcher. In 2015 he was elevated as IEEE Fellow for his contributions on "distributed power systems and microgrids.